

FLUID FLOW AND STRESSES ON MICROCARRIERS IN SPINNER FLASK BIOREACTORS

Petar LIOVIC^{1*}, Ilija D. ŠUTALO², Robert STEWART², Veronica GLATTAUER³ and Laurence MEAGHER³

¹ CSIRO Mathematics, Informatics and Statistics, Highett, Victoria 3190, AUSTRALIA

² CSIRO Materials Science and Engineering, Highett, Victoria 3190, AUSTRALIA

³ CSIRO Materials Science and Engineering, Clayton, Victoria 3169, AUSTRALIA

*Corresponding author, E-mail address: Petar.Liovic@csiro.au

ABSTRACT

The paper presents a validated CFD model for the flow in a bench-scale spinner flask that features a centrally-located magnet-driven impeller. Model development found that use of the immersed solid mesh method resulted in better correspondence with observations and μ PIV measurements than the more established sliding mesh method in ANSYS-CFX. Analysis of spatial distributions suggested stresses and turbulence in a bench-scale stirred-flask bioreactor featuring vertical outer-wall baffles were of a magnitude which could result in inhibited growth due to cell damage if the angular velocity was high enough, even when the magnitude of the Reynolds number indicated that the flow was barely turbulent.

NOMENCLATURE

N	annular velocity
D	stirrer diameter
l_k	Kolmogorov length scale
S	shear strain rate
τ	shear stress
ρ	density
μ	molecular viscosity
μ_T	eddy viscosity
ε	turbulence dissipation

INTRODUCTION

The scientific and engineering considerations associated with realizing rapid human stem cell expansion on an industrial-scale in high throughput bioreactors are varied and significant. Unlike animal cells used for therapeutic protein production, human adult stem cells (hSC) are more sensitive to culture conditions than animal cell lines (Allegrucci and Young, 2007). While high level expansion in culture of hSCs is sought in high-throughput bioreactors, it is preconditioned on minimizing variations in lineage commitment and keeping genetic and epigenetic instabilities under control. In order to achieve this in upscaled bioreactor systems the process environment in which hSC expansion occurs needs to be fully understood (Hewitt et al., 2011).

While bench-scale technology development has generated a multitude of bioreactor concepts for cultivating hSCs, the complications associated with process scale-up preclude many of these as infeasible for scale-up. Bioreactor designs that currently stand out as being

scalable are suspension bioreactors featuring microcarrier particles, which provide ample surface area for stem cell attachment and expansion within feasibly compact bioreactor volumes (Nienow, 2006). Utilization of the full surface area of the microcarriers within a bioreactor, and homogenization of the environment for stem cell expansion on the microcarrier, requires the particles to be suspended. The current preference for sustaining suspension in culture within bioreactors is mechanical agitation through stirring.

Agitation in bioreactors in the form of stirring induces flow stresses which are capable of inducing damage to stem cells and indeed to microcarriers (Croughan et al., 1987; Hewitt et al., 2011). Damage-level stresses affecting stem cell expansion are not the only concern in stirred-tank bioreactor operation for hSCs. Low shear stress levels have been noted by Cormier et al. (2006) to raise the possibility of excessive agglomeration. In addition, shear in bioreactor culture augmenting stem cell signalling has been shown to have an effect on human mesenchymal stem cell (hMSC) differentiation due to mechanisms such as mitogen activated protein kinase (MAPK) signalling, mechanotransduction, and Wnt signalling (Yeatts et al., 2012). While it is a concern, Shafa et al. (2011) note successful use of suspension bioreactors to support large-scale stem cell expansion (in their case embryonic stem cells) in a number of groups while retaining phenotype.

The distinction between shear influenced stem cell differentiation and shear induced cell damage is important, because of the flow characteristics associated with them. The stress effect in stirred-flask stem cell bioreactors and for more generic tissue engineering bioreactors tends to report shear stress levels and exposure durations to achieve a specific stem cell differentiation or stem cell expression outcome that are either single values (e.g. Glossop and Cartmell, 2009; Shafa et al., 2011; Yeatts et al., 2012), a relatively narrow-band (e.g. Zhang et al., 2011; Zhang et al., 2012), or maximum values (Cormier et al., 2006). Cormier et al. (2006) provide justification for suspension bioreactors featuring a narrow band of shear stress levels by noting a limited range for cell proliferation, based on competing considerations of shear-induced damage and agglomeration. Turbulent flow in stirred-flask bioreactors (Croughan et al., 1987; Hewitt et al., 2011), however, represents a scenario that is not characterized by a narrow band of shear stress levels. The key phenomenology of turbulence - outscatter idealized as

the self-similar breakdown of large eddies into small ones – is broad-band behaviour, as noted in the nature of the turbulent energy cascade. The cascading of characteristic shear stress magnitudes associated with a decreasing turbulent eddy length scale means that shear stresses seen by individual stem cells may be large and well beyond any narrow band associated with the mean flow. Indeed, the turbulent (Kolmogorov) microscale is postulated to be the key criterion for determining whether cell damage will occur (Croughan et al., 1987; Hewitt et al., 2011). Turbulent fluctuations at the Kolmogorov scale also affect cell attachment onto microcarriers. The effect of broad-band stresses associated with turbulence on the ability of stirred-flask bioreactor operation to preserve pluripotency in stem cells and minimize lineage commitments is poorly understood. While stirred-flask bioreactor designs that maintain laminar flow would seem the obvious way to ensure narrow-band stressing for reliable control of differentiation and lineage during stem cell expansion, scale-up that avoids a transition from laminar to turbulent flow is fanciful. Furthermore, turbulent mixing would seem to be beneficial for mediating stem cell fate by more rapidly homogenizing oxygen content (Yeatts et al. 2012) and soluble factors (Zhang et al., 2011; Zhang et al., 2012). Indeed, stirring rates typically need to be high enough to improve oxygenation through surface aeration (Croughan et al., 1987).

Scale-up of suspension bioreactors from bench scale stirred flasks to the industrial scale is not reliably done by iteration on bench-scale flasks. On the other hand, repeated testing at pilot-plant level is expensive and inefficient as an approach for testing design variations. An approach to studying stirred suspension bioreactors that enable rapid assessment of design concepts at both the bench scale and the industrial scale is Computational Fluid Dynamics (CFD) modelling. The current paper is a first study within the CSIRO stem cell bioreactor research effort towards identifying appropriate CFD models for stirred stem cell bioreactors, as well the early assessment of flow features and stress levels that will affect stem cell expansion in stirred bioreactors for hSC production.

MODEL DESCRIPTION

The ANSYS-CFX software Version 14.0 (ANSYS, Canonsburg, PA, USA) is used for the CFD modelling. Modelling choices used in the work are discussed below.

Stirrer characteristics and stirrer model choices

Three different bench-scale laboratory glassware options are of interest to the pre-scale-up phase of the CSIRO research effort into stirred suspension bioreactors – the BellCo[®] flask, the Corning[®] flask, and the Techne[®] flask. Figure 1 shows CAD designs of each flask type. The BellCo flask features a large magnet-driven impeller that spins on a vertical axis (1 rotational degree-of-freedom (DOF)), and relies on a large impeller blade that spans most of the radius of the flask to achieve suspension. The Corning flask features a magnet-driven impeller that spins on a vertical axis that is not as wide as that in the BellCo flask, but does feature baffles to promote mixing. The Techne flask features a rod stirrer that is attached by magnetic force to the top of the flask, and the stirrer undergoes 3 DOF rigid body rotation based on both magnetic forces (from the plate the flask sits on) and fluid-structure interaction (FSI) within the flask.

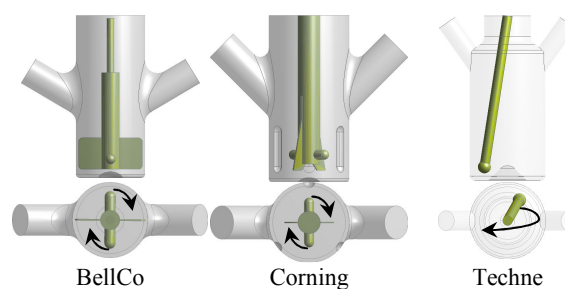


Figure 1: Different bench-scale stirred-flask bioreactors (top row), and bird-eye views showing stirrer trajectory relative to flask outer walls (bottom row). The BellCo and Corning impeller motion is pure rotation, while the Techne stirrer rod motion is a more arbitrary 3 DOF rotation about the flask lid pivot.

Presentation of these three laboratory glassware choices for the bench-scale stirred-flask bioreactor is important for the choices of stirrer model considered in the work. The sliding-mesh method for achieving stirrer modelling is fine for problems where the stirrer motion is naturally confined within the core of the flask, and is a reasonable choice for the Corning flask. However, the sliding-mesh method is not necessarily well suited to the BellCo and Techne flasks, because of the very close proximity to which the stirrers can come to the side wall or the bottom mound. For an alternative treatment of the stirrer, the ANSYS-CFX software Version 14.0 software features an immersed solid modelling capability. As a first application of CFD to stirrer-flask bioreactors, the current work features a comparison of the relative performance of the sliding-mesh method and the immersed-solid method on the problem of the Corning flask bioreactor, for which both methods should be valid.

Other model features

Typical laboratory stirred-flask bioreactor operation features only partially-filled flasks, with culture levels just above the impeller blades in Figure 1. Typical protocols also involve stirrer speeds that are moderately low: up to 60 rpm and usually lower, such that free surface deformations are low. Such operating conditions enable the free surface to be realistically modelled as a rigid free-slip boundary (rather than generated as part of the solution), simplifying the CFD to a single-phase model. Early video evidence suggests the imposition of a flat rigid free surface to be reasonable under the flow conditions under consideration. In the first instance for establishing the fundamental features of the CFD model and the fluid flow, the microcarrier particles are neglected. Turbulence models considered in this study include the $k-\omega$ model, the BSL-RSM model, and the LES-WALE model; the theory and implementation of these turbulence models in CFX Version 14.0 is described in the software documentation.

EXPERIMENTAL

Micro-PIV system

A Nd:YAG double-pulsed laser system (NEW WAVE minilase-3/15 Hz, each with 5 ns pulse length) was used for the PIV system. A Hall Effect Switch (A1120, Allegro Microsystems) was attached to the magnetic stirrer, so that it switched on and off as a result of the oscillating magnetic field created by the stirrer. The resulting signal

was input into an oscilloscope (Rigol, DS5062MA) so that the impeller angular speed could be measured, and the signal was also fed into a custom-built laser and camera triggering system. The system allowed the time between laser pulses to be changed and the position of the impeller in an image to be varied. A Kodak_Megaplus_ES_1.0-TH camera was used and images were captured on a PC, before analysis with DynamicStudio v3.20.0 (Dantec).

Experimental setup

Figure 2 shows a photograph of the Corning flask mounted in the μ PIV system. The flask was rotated to enable the laser sheet to pass through the flask unimpeded by either the arms of the flask or by the baffles; Figure 3 shows the orientation of the laser sheet relative to the internal features of the flask. The triggering mechanism in the μ PIV system was set to generate velocity vector maps when the magnets on the impeller were coplanar with the laser sheet. The instantaneous velocity vector maps were then averaged to generate an ensemble-averaged velocity vector map for the instant per half-period of rotation of the impeller where the magnets on the impeller aligned with the laser light sheet. For an angular velocity of 60 rpm stirring a culture bath of quiescent depth 36.4 mm, the experimental vector map to one side of the impeller shaft is shown in Figure 4. [The impeller Reynolds number $Re=ND^2/\nu$ is ~ 1250 , based on $D=35$ mm.]

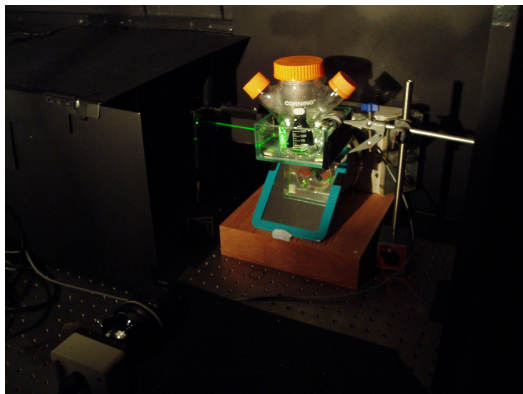


Figure 2: Corning flask within micro-PIV system.

The PIV velocity vector map (Figure 4) shows two main vortices – a main lower vortex underneath the magnet level, and a main upper vortex which is radially further out from the magnet and above the magnet level. Smaller vortices are located near the top of the image in Figure 4 i.e. just underneath the free surface – one adjacent to the impeller shaft, and the other adjacent to the outer wall.

CFD MODEL VALIDATION

Grid dependence study

As a first assessment of grid dependence, the sliding-mesh CFD model was run with the $k-\omega$ turbulence model, and mesh deformation was enabled. Three meshes – low, medium and high -- were used in the grid-dependence study (12000, 186000 and 542000 elements, respectively). The velocity vector maps generated by the sliding-mesh CFD model with the $k-\omega$ turbulence model are visually similar to the PIV result in Figure 4. Figure 5 alternatively shows streamlines which identify major vortices, as well as velocity component value distributions, in order to

better identify any differences due to grid-dependence effects. Comparing against the high-resolution solution, the low-resolution solution does not resolve the flow structure in the upper half of the flow that is predicted by both the medium- and high-resolution simulations. Comparisons between the medium- and high-resolution result illustrate more subtle differences, but overall the solutions are similar in structure and intensity. The result supports the notion that the medium-resolution mesh for the sliding-mesh CFD models results in a flow solution close to the grid-independent solution. [This assessment is mainly relevant to the sliding-mesh CFD approach; simulation using the immersed solid approach for the stirrer modelling is less computationally intensive, allowing for the feasible use of larger meshes. (Just under 1 million elements are used in the immersed solid CFD model in the current work.)]

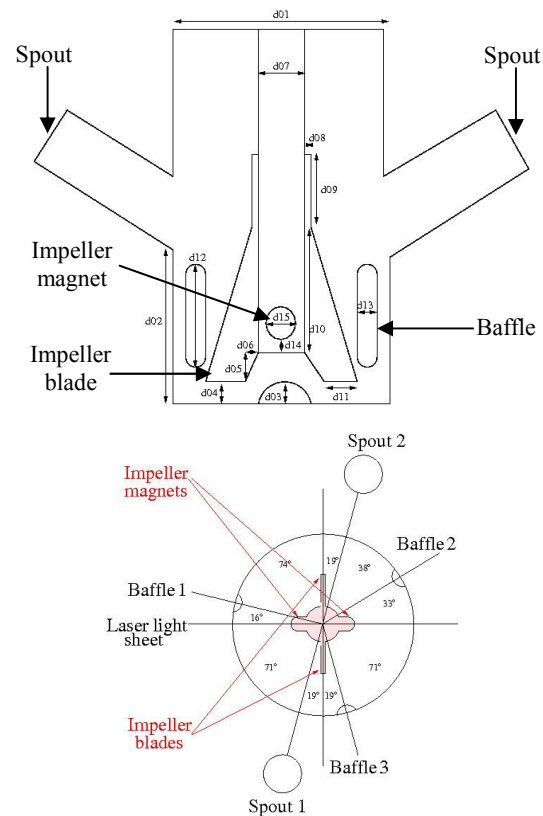


Figure 3: Corning flask CFD model geometry setup. (Top) Positioning of impeller within flask and positioning of baffles (refer to Table 1 for lengths). (Bottom) Orientation of laser light sheet relative to baffles, and orientation of impeller used for ensemble-averaging for velocity imaging in vertical plane through centre of Corning flask. The geometry specification is completed by truncating the domain with a flat free-slip wall to represent the free surface at a height of 36.4 mm above the bottom.

Geometry parameter	Length (mm)	Geometry parameter	Length (mm)	Geometry parameter	Length (mm)
d01	65	d06	1	d11	10
d02	52.5	d07	18	d12	38
d03	4	d08	0.5	d13	10
d04	7.5	d09	20	d14	3.5
d05	5	d10	35	d15	8

Table 1: Geometry parameters in Corning flask.

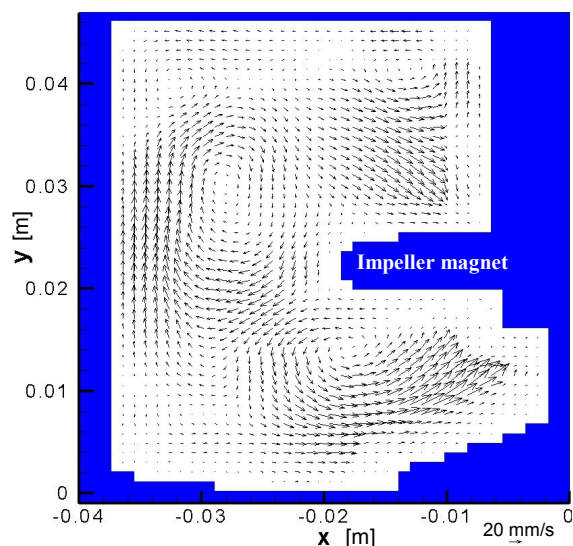


Figure 4: Experimental ensemble-averaged velocity vector map at laser light sheet location shown in Figure 3, generated by the μ PIV system for the case of 60 rpm impeller speed. The reference vector magnitude (bottom of plot) is 20 mm/s.

Comparison with μ PIV data

In comparison to the experimental result in Figure 4, the streamlines shown in Figure 5, at first glance, capture the lower vortex and the mid-level near-magnet vortex quite well. Some attempt is made in that sliding-mesh k - ω model to capture the vortical structure high up in the flask liquid, but its extent seems well overpredicted. It would appear that this large-upper-vortex prediction is unique to the combination of the k - ω model with the sliding mesh method, with the other CFD models tested failing to capture any vortical structures above the mid-level vortex, instead predicting largely laminar flow. The result shown in Figure 6(c), where the k - ω model is used but the stirrer modelling is done using the immersed solid method, is intriguing because the differences between Figures 6(a) and 6(c) are solely due to the use of the immersed-solid method in preference to the sliding-mesh method.

Comparison with the PIV data shows that no single CFD model tested in the work achieved full correspondence in all vortical structures in the laser light sheet plane, but that all the CFD models do capture the two main vortices shown in Figure 4. A first assessment of the relative quality of CFD models for the Corning stirred-flask uses the distance of the relevant vortex centre away from the vortex centre locations seen in the PIV. Table 2 shows the immersed solid CFD model to get quite close to the main mid-level vortex. Another assessment of the relative quality of the CFD models is based on velocity profiles. For valid comparison given the difference in the locations of the vortex centres between models, the lines along which the profiles are extracted are placed to pass through the vortex centre locations captured in each model. Figure 7 shows that the models pick up the general trends in velocity profiles moving away from the vortex centres, but with larger errors well away from the vortex centres as differences in flow structure between models become more pronounced. Overall for the velocity variation behaviour between the local extrema in velocity either side of the relevant major vortex, the immersed solid CFD model seems to be able to best represent the PIV data.

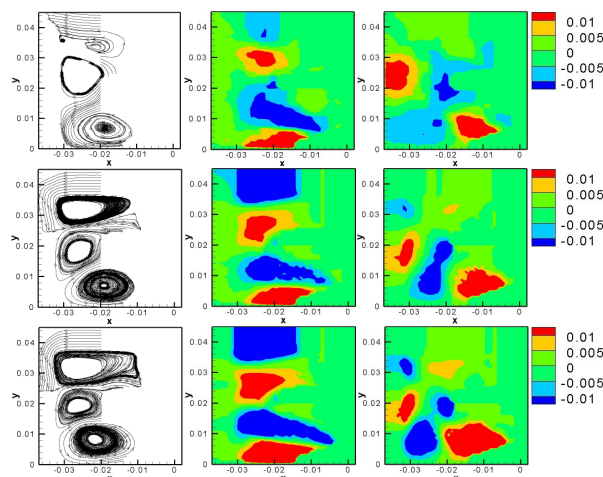


Figure 5: Results of grid-dependence study using the sliding-mesh CFD model of the Corning stirred-flask and the k - ω turbulence model, for the flow field in the plane of the PIV light sheet: (left column) streamlines; (middle column) u -velocity component; (right column) w -velocity component; (top row) low-resolution mesh; (middle row) medium-resolution mesh; (bottom row) high-resolution mesh.

Comparison with the PIV data shows that no single approach tested in this work does an acceptable job of capturing the flow structure just underneath the free surface. Even though the 60 rpm stirrer speed does not cause substantial free surface deformation, the ability of the free surface to accommodate even slight deformation is known to be important in modifying turbulence structure due to interface/turbulence interactions. As such, CFD models with rigid free-surface representations should not be expected to capture or impose the correct near-interface turbulence asymptotics. Proceeding in this work with the immersed solid CFD model of the Corning stirred flask, it is worth noting that immersed solid model cannot be used in conjunction with the multiphase flow modelling in CFX. Until this situation is corrected in future CFX releases, it is uncertain whether any of the existing CFX models tested in this work can be modified adequately to correctly capture the near-free-surface vortices seen in the PIV result in Figure 4.

FLOW ANALYSIS

Shear stress, Kolmogorov length scale

For CFD models featuring eddy viscosity-based turbulence models, the shear stress experienced by a microcarrier particle at any location is approximated as

$$\tau = (\mu + \mu_T)|S|, \quad (1)$$

while the Kolmogorov length scale is computed as

$$l_k = (\mu^3 / (\rho^3 \varepsilon))^{1/4}. \quad (2)$$

Figure 8(a) shows the shear stress distribution in the PIV light sheet at an instant when the magnets are aligned with the light sheet. It turns out that the magnet ends are the locations in the entire flow featuring the highest shear stress levels at this instant in time. This is not surprising since the magnet protrudes out further than the blades of the impeller. While the magnet ends are also regions of high turbulence as denoted by locally low values of l_k (hence high turbulence dissipation), the global minimum value of l_k is actually on the baffle surface. In the instant shown in Figure 8, the global minimum for l_k is 75 μ m.

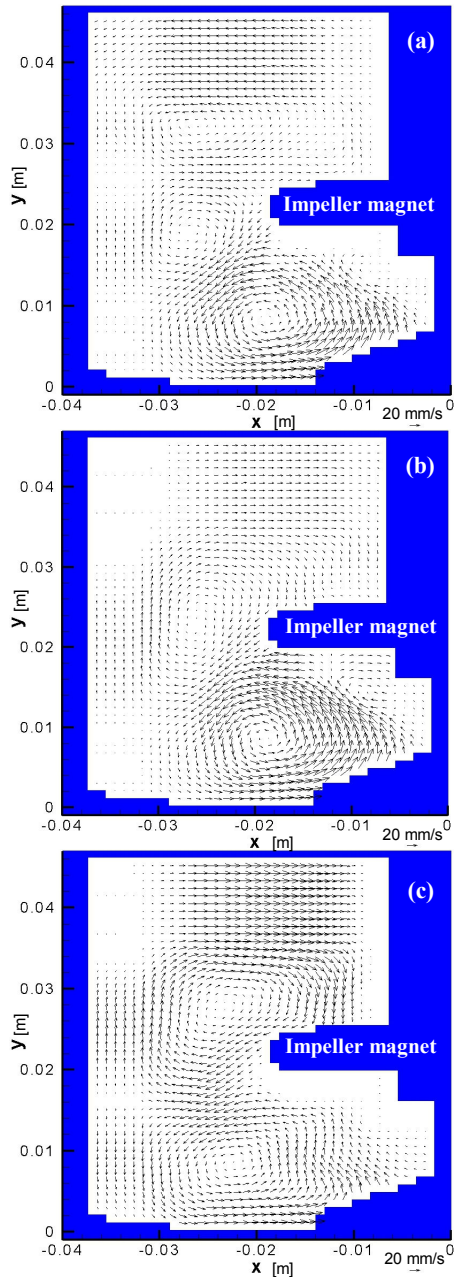


Figure 6: Predicted ensemble-averaged velocity vector maps in plane of PIV light sheet: (a) sliding mesh, medium-res, $k-\omega$ model; (b) sliding mesh, medium-res, BSL-RSM model; (c) immersed solid, high-res, $k-\omega$ model. The vector map in Figure 4 is the appropriate experimental comparison.

During operation of the Corning stirrer-flask according to protocols to achieve particle suspension, the minimum Kolmogorov length scale will typically be lowest when an impeller magnet passes a baffle. Larger regions of relatively low l_k (less than $125 \mu\text{m}$) occur in the wakes of the impeller blades. The l_k in the wakes of the impeller blades may be more important than the global minimum. This is because most microcarrier particles will pass through the impeller blade wakes during a protocol where impeller motion only occurs periodically to induce particle suspension, while fewer particles will pass in close proximity to the tip of the impeller magnet.

Case	Vortex Centre x-coord	Vortex Centre y-coord	Distance from PIV vortex centre
Main Lower Vortex			
PIV	-18.2	13.9	
No turbulence model	-19.5	7.2	6.8
$k-\omega$	-19.1	7.2	6.8
BSL-RSM	-19.0	8.5	5.5
LES-WALE	-18.3	7.7	6.2
ImmSol $k-\omega$	-22.3	8.4	6.8
Main Upper Vortex			
PIV	-28.0	29.6	
No turbulence model	-25.7	19.5	10.4
$k-\omega$	-26.1	18.1	11.7
BSL-RSM	-26.1	22.7	7.2
LES-WALE	-25.7	21.8	8.1
ImmSol $k-\omega$	-23.6	27.8	4.8

Table 2: Locations of vortex centres in plane of PIV light sheet generated by different transient CFD models of the Corning stirred-flask. (Black data: sliding mesh method; grey data: immersed solid (ImmSol) method.) [mm units.]

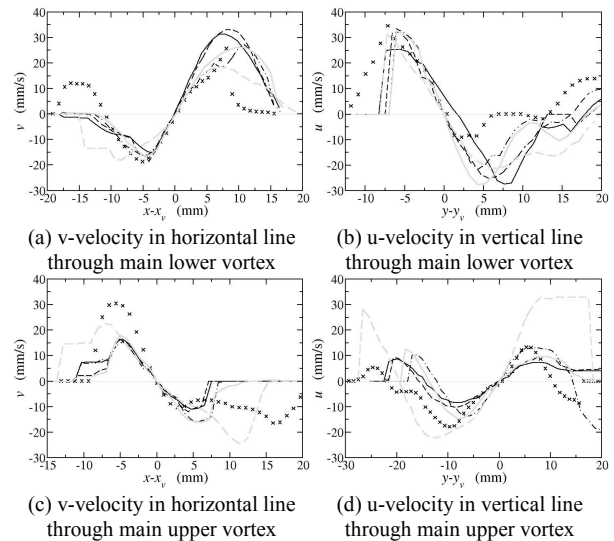


Figure 7: Velocity component magnitude profiles vector maps in plane of PIV light sheet generated by transient CFD models of the Corning stirred-flask: \times PIV; — sliding-mesh + no turbulence model (MILES); - - - sliding-mesh + $k-\omega$; — sliding-mesh + BSL-RSM; - - - sliding-mesh + LES-WALE; - - - immersed-solid + $k-\omega$.

Turbulence, cell damage and microcarrier suspension

The results in Figure 8 feature shear stress and Kolmogorov length scale magnitudes similar to those featured in the microcarrier-based suspension bioreactor literature. The most interesting of these results is from Croughan et al. (1987) regarding the dependence of the relative cell growth on l_k , in which the growth of human FS-4 cells varied abruptly with l_k , from 100% growth at $l_k > 135 \mu\text{m}$, down to 60% growth at $l_k \approx 115 \mu\text{m}$, 20% growth at $l_k \approx 100 \mu\text{m}$, and ultimately zero growth at $l_k \approx 90 \mu\text{m}$. For the time instant shown in Figure 8(b), it is apparent that half of the flow plane at magnet level will feature some inhibition of cell expansion, but substantial inhibition occurs in only the small proportion (5-10 %) of the flow plane that is in the wakes of the magnets and the impeller blades.

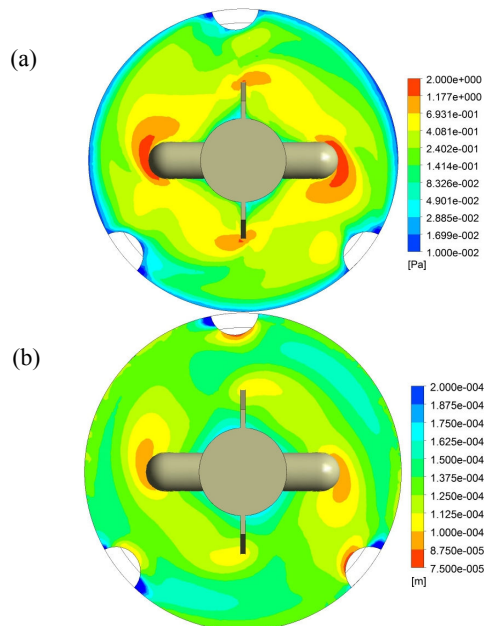


Figure 8: Distribution acting on microcarrier particle surfaces by the fluid flow during operation of the Corning stirred-flask at 60 rpm, as predicted by the immersed solid CFD model in the plane 20 mm above the flask base (magnet level) at one instant of the operation: (a) shear stress; (b) Kolmogorov length scale.

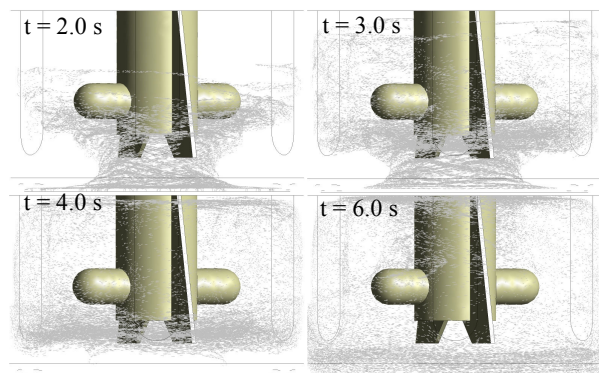


Figure 9: Sample evolution of particle suspension to firstly achieve a just-suspended state, and then to a more homogenized state upon entrainment of particles into the flow structures. [Impeller location shown at $t = 6.4$ s.]

A true time- and volume-averaged measure of the relative cell growth depends on microcarrier history tracking, and logging to tally the stress exposures as the microcarriers pass through different parts of the flow. A first clue to the effect of flask spin-up on potential stem cell death is given in Figure 9, generated by adding Lagrangian particle tracking into the immersed solid CFD model. [This result is only for qualitative illustrative purposes, given the current capability of CFX to correctly model particle interactions with the immersed solid representation of the stirrer is unproven.] The frames in Figure 9 indicate that spin-up to achieve full suspension throws the particles into the high-stress zones in the wakes of the magnets and impeller blades, but that particles later move out of the high-stress zones as the particle distribution stabilizes in the mean stirrer-driven flow. The short time exposure of the majority of the microcarrier population to these regions may spare wholesale cell damage. For quality-control purposes and for avoiding lineage control

problems, however, the evidence of interaction of a significant proportion of the microcarrier population with the high-stress regions in Figure 8 is of some concern.

CONCLUSION

The paper presents a CFD model that is shown to be a realistic model of the hydrodynamics within a Corning stirred-flask. The CFD models feature room for improvement through targeted improvements to turbulence modelling, stirrer motion modelling and free surface modelling. The work shows CFD to be useful in identifying possibilities for microcarrier exposure to regions of stress levels that could cause cell damage and stem cell differentiation issues. As such, CFD shows promise for use as risk-mitigation tool prior to commissioning protocols used in for stem-cell bioreactors.

ACKNOWLEDGEMENTS

This work was supported by the Biomedical Materials and Devices Theme of CSIRO Materials Science and Engineering (CMSE).

REFERENCES

- ALLEGRUCCI, C., and YOUNG, L.E., (2007), "Differences between human embryonic stem cell lines", *Hum. Reprod. Update*, **13**, 103-120.
- CORMIER, J.T., ZUR NIEDEN, N.I., RANCOURT, D.E., and KALLOS, M.S., (2006), "Expansion of undifferentiated murine embryonic stem cells as aggregates in suspension culture bioreactors", *Tissue Eng.*, **12**, 3233-3245.
- CROUGHAN, M.S., HAMEL, J.-F., and WANG, D.I.C., (1987), "Hydrodynamic effects on animal cells grown in microcarrier cultures", *Biotech. Bioengr.*, **29**, 130-141.
- GLOSSOP, J.R., and CARTMELL, S.H., (2009), "Effect of fluid flow-induced shear stress on human mesenchymal stem cells: differential gene expression of IL1B and MAP3K8 in MAPK signaling", *Gene Expr. Patterns*, **9**, 381-388.
- HEWITT, C.J., LEE, K., NIENOW, A.W., THOMAS, R.J., SMITH, M., and THOMAS, C.R., (2011), "Expansion of human mesenchymal stem cells on microcarriers", *Biotechnol. Lett.*, **33**, 2325-2335.
- LIOVIC, P., LAKEHAL, D., (2007), "Multi-physics treatment in the vicinity of arbitrarily deformable gas-liquid interfaces", *J. Comput. Phys.*, **222**, 504-535.
- SHAFI, M., KRAWETZ, R., ZHANG, Y., RATTNER, J.B., GODOLLEI, A., DUFF, H., and RANCOURT, D.E., (2011), "Impact of stirred suspension bioreactor culture on the differentiation of murine embryonic stem cells into cardiomyocytes", *BMC Cell Biol.*, **12**, 53-64.
- YEATS, A.B., CHOQUETTE, D.T., and FISHER, J.P., (2012), "Bioreactors to influence stem cell fate: augmentation of mesenchymal stem cell signalling pathways via dynamic culture systems", *Biochimica Biophysica Acta*, **in press**.
- ZHANG, H., DAI, S., BI, J., and LIU, K.-K., (2011), "Biomimetic three-dimensional microenvironment for controlling stem cell fate", *Interface Focus.*, **1**, 792-803.
- ZHANG, H., KAY, A., FORSYTH, N.R., LIU, K.-K., and EL HAJ, A.J., (2012), "Gene expression of single human mesenchymal stem cell in response to fluid shear", *J. Tissue. Eng.*, **3** (1), 2041731412451988.